Grouping of carbonaceous nanomaterials based on association of patterns of inflammatory markers in BAL fluid with adverse outcomes in lungs

Naveena Yanamala, Ishika C. Desai, William Miller, Vamsi K. Kodali, Girija Syamlal, Jenny R. Roberts & Aaron D. Erdely

View supplementary material

Accepted author version posted online: 08 Jul 2019.
Published online: 30 Jul 2019.

Submit your article to this journal

Article views: 88

View related articles

View Crossmark data

Taylor & Francis
Taylor & Francis Group

ARTICLE

Check for updates

Grouping of carbonaceous nanomaterials based on association of patterns of inflammatory markers in BAL fluid with adverse outcomes in lungs

Naveena Yanamala[a]*, Ishika C. Desai[a,b], William Miller[c], Vamsi K. Kodali[a], Girija Syamlal[c], Jenny R. Roberts[a] and Aaron D. Erdely[a]

[a]Health Effects Laboratory Division, National Institute for Occupational Safety and Health, Morgantown, WV, USA; [b]Department of Molecular Genetics, The Ohio State University, Columbus, OH, USA; [c]Respiratory Health Division, National Institute for Occupational Safety and Health, Morgantown, WV, USA

ABSTRACT

Carbonaceous nanomaterials (CNMs) are universally being used to make commodities, as they present unique opportunities for development and innovation in the fields of engineering, biotechnology, etc. As technology advances to incorporate CNMs in industry, the potential exposures associated with these particles also increase. CNMs have been found to be associated with substantial pulmonary toxicity, including inflammation, fibrosis, and/or granuloma formation in animal models. This study attempts to categorize the toxicity profiles of various carbon allotropes, in particular, carbon black, different multi-walled carbon nanotubes, graphene-based materials, and their derivatives. Statistical and machine learning-based approaches were used to identify groups of CNMs with similar pulmonary toxicity responses from a panel of proteins measured in bronchoalveolar lavage (BAL) fluid samples and with similar pathological outcomes in the lungs. Thus, grouped particles, based on their pulmonary toxicity profiles, were used to select a small set of proteins that could potentially identify and discriminate between the toxicity profiles associated within each group. Specifically, MDC/CCL22 and MIP-3β/CCL19 were identified as common protein markers associated with both toxicologically distinct groups of CNMs. In addition, the persistent expression of other selected protein markers in BAL fluid from each group suggested their ability to predict toxicity in the lungs, i.e. fibrosis and microgranuloma formation. The advantages of such approaches can have positive implications for further research in toxicity profiling.

1. Introduction

Over the past two decades, the field of nanotechnology – aimed to design, characterize, and produce materials on a nanometer scale – has been fast growing and has revolutionized many aspects of our lives. The incorporation of engineered nanoparticles (NPs) in products used in various industries (e.g. electronics, manufacturing, construction, energy); consumer products (e.g. cosmetics, food packaging) and biomedicine p oses an increased risk of exposure in humans. Incidental human exposure to carbonaceous nanomaterials (CNMs) can occur via treatment of various diseases, as well as through their presence in manufacturing, occupational, and

environmental settings. Studies of short-term and prolonged exposure to CNMs, especially carbon nanotubes, revealed adverse outcomes in the lungs such as inflammation, fibrosis, and formation of granulomas in animal models (NIOSH-CIB-65 2013), suggesting the significance of understanding the toxicity of CNMs in protecting those exposed. It is near impossible to test the biological outcomes of all of the CNMs, which includes both pristine material and alterations that may occur along the life cycle of the particle, because of the time and expense required to do so. Developing models to forecast and group NPs based on toxicity responses and the additional factors that impact such outcomes would

aid in overcoming the need to assess the toxicity of each novel NP in a laboratory.

Several considerations have recently been made to offer frameworks to group or categorize NPs (Kuempel et al. 2012; Oomen et al. 2014; Arts et al. 2015; Godwin et al. 2015; Arts et al. 2016; Braakhuis, Oomen, and Cassee 2016). Grouping has been based on some combination of exposure and use scenarios, intrinsic and system-dependent properties, and toxicity end-points *in vitro* or *in vivo*. While these approaches may be sufficient for effective grouping of NPs, they do not necessarily address specific mechanisms associated with NP toxicity and pathology. Complications to current hazard ranking and generalized mechanisms of toxicity of grouped engineered nanomaterials include methodological inconsistency, variance in, or missing, end-points across studies considered by different groups for evaluating toxicity responses of NPs, as well as the lack of precise understanding of the role of different NP characteristics on various biological responses.

This study presents a statistical/machine-learning based approach to group together CNMs, in particular carbon black, multi-walled carbon nanotubes (MWCNTs), grapheme, and their derivatives. To accomplish the goal, a consistent feature that was measured in all samples was prioritized. In this case, a panel of proteins measured in lung bronchoalveolar lavage fluid following exposure was utilized. As a first step, before selecting proteins that could discriminate the responses to different types of CNMs, a hierarchical cluster analysis was performed to group CNMs based on similarities in their pulmonary toxicity profiles. Following this, a latent cluster analysis was performed to see whether similar groupings of various CNMs would emerge based on histopathological alterations in lungs. In a recent study from our group, we have shown that a sparse classification algorithm would be optimal in selecting protein markers that can predict biological or exposure effects to MWCNTs (Yanamala et al. 2018). To further extend the applicability of the previous presented methodology and approach for MWCNTs to other CNMs, we applied a classification algorithm to select protein markers to distinguish between the different groups (e.g. carbon nanotubes, graphene-based materials, and carbon black). This further led to identification of potential markers

through which CNMs could affect the lung and induce pulmonary toxicity responses, thus allowing for meaningful grouping of CNMs based on adverse outcomes in lungs.

2. Materials and methods

2.1. Data selection and pre-filtering/processing

The data used in this study were collected from various studies (Roberts et al. 2015; Bishop et al. 2017; Roberts et al. 2018; Yanamala et al. 2018) conducted at the National Institute for Occupational Safety and Healthy (NIOSH), Centers for Disease Control and Prevention (CDC). All studies referenced in the paper were conducted in the AAALAC International accredited NIOSH animal facility in accordance with the NIOSH Institutional Animal Care and Use Committee. In this study, the various training datasets employed consisted of pristine graphenes of various lateral dimensions (Gr1 – 1 μm; Gr5 – 5 μm; Gr20 – 20 μm), graphene oxides (GO – 5 μm), reduced graphene-oxide (rGO – 5 μm), pristine as-produced MWCNT (MW-#3, MW-#2), their polymer-coated counterparts (MW-#3-PC, MW-#2-PC), MW-#5 (Mitsui-7; MWCNT-7), and carbon black (CB – is Printex 90 Degussa). All graphene-based materials including Gr1, Gr5, Gr20, GO, and rGO were provided by Cabot Corporation, Billerica MA. Multi-walled carbon nanotube based materials were generously provided by two companies within the United States as reported previously (Bishop et al. 2017). This panel of CNMs were chosen considering variability in particle characteristics such as shape, size, and surface modifications as well as presence or absence of adverse pathological outcomes such as fibrosis or (micro-)granulomatous lesions.

Data corresponding to a panel of ∼51 to 54 proteins in the acellular first fraction of brochoalveolar lavage (BAL) fluid collected from male C57BL/6J mice exposed by oropharyngeal aspiration to 4 and 40 μg of each particle by various researchers at NIOSH were obtained. The pathogen-free male C57BL/6J mice, 8–10 weeks of age and weighing 20–25 g, were obtained from Jackson Laboratories (Bar Harbor, ME). Data from a total of 260 animals with an $n \geq 5$ animals per group (12 particles * 2 time points * 2 doses * 5 animals/group + 20 vehicle-exposed controls = 260 animals) were

considered for analysis. The vehicle, physiological dispersion media (DM), contained mouse serum albumin (0.6 mg/mL) and 1,2-dipalmitoyl-sn-glycero-3-phosphocholine (DPPC; 0.01 mg/mL) and was prepared in United States Pharmacopeia (USP)-grade phosphate-buffered saline (PBS) without calcium and magnesium. Following the collection and pooling of data from different experimental groups, all data were standardized, pre-filtered and normalized. As a preliminary measure, proteins lacking data at all exposure levels were eliminated from the dataset. Proteins with values below the limit of detection were replaced with values equal to half of the lower limit of quantification values (LLOQ). This resulted in the evaluation of 46 proteins at 1 and 28 d post-exposure. The pre-filtered data was then normalized by comparing the raw values to their corresponding controls for each time point and exposure level. This resulted in fold change values, which were further log_2-transformed for the final analysis.

2.2. Hierarchical cluster analysis

To identify clusters of carbonaceous nanomaterials with similar inflammatory responses, a hierarchical cluster analysis was performed in BAL fluid proteins at 24 h and 28 d post-exposure to various MWCNTs, graphenes, and their derivatives. This analysis also included responses upon exposure to carbon black (CB). RStudio (RCoreTeam 2014) was used to perform a hierarchical clustering analysis of the samples respective to protein exposure and time point in BAL fluid from mice exposed to various nanomaterials. This was done using hclust() function in R via Euclidean distance similarity between samples, and by utilizing ward.D2 linkage between members of the clusters. Merging this information allowed for the creation of heat maps, with shades of colors corresponding to relative expression levels of the proteins at each time point and exposure level. The heat maps and clusters were created using package heatmap for R (RCoreTeam, 2014).

2.3. Latent class analysis (LCA)

A cluster analysis was applied to the histology data as observed at endpoints of 60 or 84 d post-exposure to CNMs from corresponding studies (Roberts et al. 2015; Bishop et al. 2017) using the latent class model (Collins and Lanza 2010), a special type of finite-mixture modeling (McLachlan and Basford 1988) which allows one to base the clustering on a statistical model rather than on an algorithm. The latent class model assumes that the association between some observed categorical variables can be explained by the existence of mutually exclusive latent classes. The key assumption for the model is that there is conditional or local independence, given the assignment of the observations to latent classes. LCA is sometimes viewed as a type of factor analysis for categorical data, but it can also be viewed as a type of cluster analysis, where an assignment procedure minimizes the number of incorrect assignments for the latent class model (Goodman 2007). The Akaike information criterion (AIC) and the Bayesian information criterion (BIC) are used to determine the number of LCA classes or clusters. Although there is no general agreement about the relative value of these two criteria, the number of clusters determined by minimizing the BIC statistic is generally more conservative (i.e. recommends fewer clusters).

The latent class model was fitted using the freeware procedure PROC LCA (Lanza et al. 2015) which was written to work with SAS® software (SAS-Institute 2004). The pathology data considered for LCA are from studies (Roberts et al. 2015; Bishop et al. 2017) where histology slides were quantitatively analyzed by certified veterinary pathologists at Charles River Laboratories (Frederick, MD), who have been blinded to the different treatment groups (Roberts et al. 2015; Bishop et al. 2017). Indices of inflammation, and fibrosis were scored on scale of 0–5, where 0 = no observed effect, 1 = minimal response, 2 = mild response, 3 = moderate response, 4 = marked response, and 5 = severe response. The final dataset has a total of 129 animals which are nested within the 24 primary sampling units (i.e. samples collected at 2 different doses from mice exposed to 12 different CNM particles), or approximately five animals per sampling unit. In order to use these in the analysis, the 'clusters' option in PROC LCA was invoked. Bayes theorem is applied to the modeling results to calculate the posterior class probabilities, which estimates the probability that an assignment to a latent class is correct, conditional

on the response probabilities determined by the model.

2.4. Sparse supervised machine learning-based classification for selection of protein markers

The data, consisting of explanatory variables, fold changes, and class variables as '1' or '2' corresponding to type of exposure or exposed versus vehicle-exposed controls in each case, was used as input to the algorithm. For this dataset, samples in one group were labeled with a '1', while samples in a second group were labeled with a '2'. A sparse supervised classification algorithm known as 'lone-star' was applied to the data to identify proteins in lung lavage fluid that can distinguish between control and exposed groups. 'Lone-star,' or "l_1-, l_2-norm support vector machine (SVM) t-test with RFE' algorithm has been described previously and successfully applied to various cancer-related issues, as well as been used to identify MWCNT exposure and/or toxicity (Vidyasagar 2014; Misganaw et al. 2015; Ahsen et al. 2017; Yanamala et al. 2018). This algorithm was selected based on its intrinsically beneficial SVM characteristics, as well as its ability to select correlated features independent of noise and redundancy regardless of varying dataset sizes. The lone-star algorithm implements several machine learning ideas such as combined l_1-, l_2- norm SVM (Bradley and Mangasarian 1998), stability selection (Meinshausen and Bühlmann 2010), and recursive feature elimination (Guyon et al. 2002) to overcome such problems and identifies a small number of highly predictive features. Further details corresponding to the algorithm and the precise parameters employed can be found in previous studies (Ahsen et al. 2017; Yanamala et al. 2018). Application of this algorithm on each dataset resulted in a set of proteins that could potentially differentiate between the classes under comparison, as well as the estimated percentage of correctly classified samples. The use of never seen test data was used to assess the overall performance and accuracy of the different classification models in predicting new data, potentially avoiding over-fitting. The external validation test set considered for performance evaluation included protein concentrations in BAL fluid samples from C57BL/6 mice exposed to vehicle (i.e. DM), 4 and 40 μg of Gr5 and

Table 1. Independent validation of the selected predictive markers.

Classification model	Details of TestDataSet	Prediction accuracy (external-validation)	Sensitivity	Specificity
DM versus group 1	Testset1	90.0	80.0 (DM)	100.0 (MW#5)
DM versus group 2	Testset2	92.0	80.0 (DM)	100.0 (Gr5)
Group 1 versus group 2	Testset3	100.0	100.0 (MW#5)	100.0 (Gr5)

The prediction accuracies and performance evaluation measures using independent datasets with protein fold changes from lung lavage fluid from C57BL6 mice upon aspiration exposure to vehicle (e.g. DM), 4 and 40 μg of Gr5 and 40 μg of MW#5 (i.e. Mitsui-7). The animals were sacrificed on days 1 and 28 following last day of exposure. Specificity corresponds to $TN/(TN + FP)$, sensitivity to $TP/(TP + FN)$ and accuracy is determined as $(TP + TN)/(TP + FP + TN + FN))$ (*TN: true negatives; FN: false negatives; TP: true positives; FP: false positives).

40 μg of MW#5 and were sacrificed at days 1 and 28 post-exposure (Roberts et al. 2015; Yanamala et al. 2018). Three subsets (Supplemental Table S2) containing data from vehicle-exposed mice alone with those representing high dose (40 μg) exposure to MW#5, testset1, exposure to both (4 and 40 μg) concentrations of Gr5, testset2, and all samples exposed to both Gr5 and MW#5 without controls or vehicle-exposed mice, testset3, were created to evaluate and assess the performance of the generated models in classifying the new test data (Table 1).

3. Results

3.1. Hierarchical cluster analysis identified groups of nanoparticles with similar inflammatory responses

A hierarchical clustering analysis (HCA) was performed to distinguish or discriminate the inflammatory responses induced by different types of multi-walled carbon nanotubes (MW-#5, MW-#3, MW-#3-PC, MW-#2, MW-#2-PC, graphene-based materials (graphene [Gr1, Gr5, Gr20], graphene oxide [GO], and reduced graphene oxide [rGO]), and carbon black (CB). HCA (unlike model-dependent analyses of supervised machine learning methods) is a model-free statistical approach that makes no a priori assumptions about the class identification of data. The resulting dendrogram from HCA analysis of a total of 46 proteins in BALF at 1 and 28 days post oropharyngeal aspiration exposure to different nanoparticles considered is presented in Figure 1. The heat maps show areas of protein upregulation
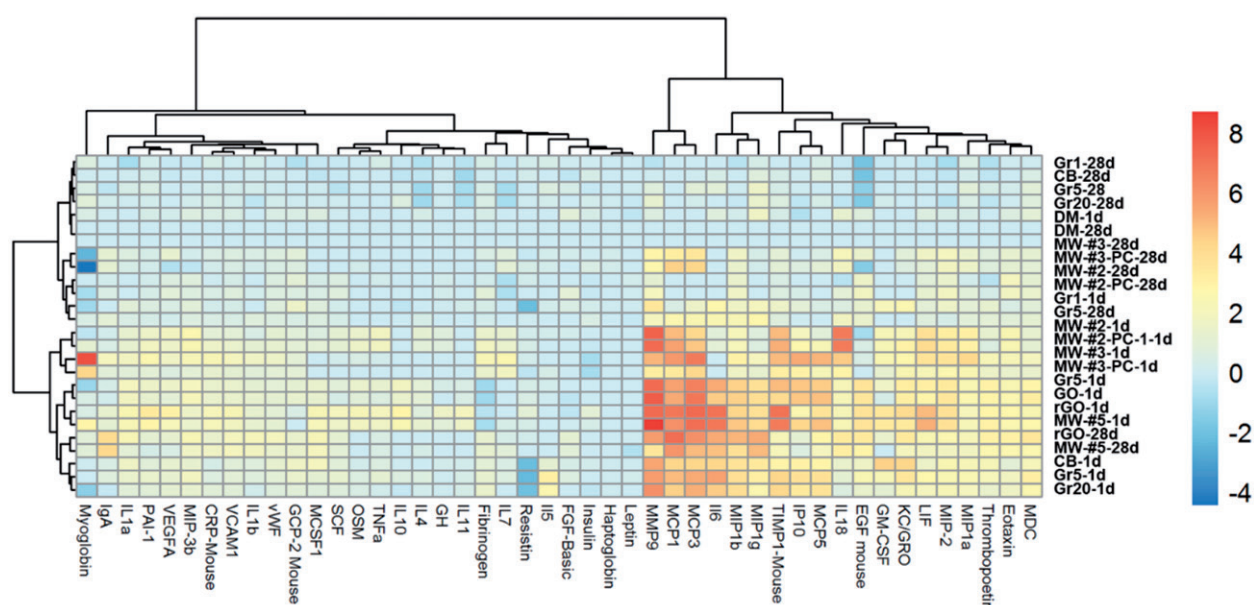
Figure 1. Hierarchical cluster analysis of proteins in BAL fluid of mice exposed to various graphene based materials, MWCNTs, and carbon black. The samples of BAL fluid in mice exposed to 40 μg/mouse concentrations of various CNMs studied along with respective controls were clustered based on the Euclidean distance metric and ward.D2 clustering method at 24 h and 28 da post-exposure. The heat map presents relative $\log_2$-transformed fold change values of proteins, increasing from blue to red. The dataset consisted of responses upon exposure to pristine graphenes of various lateral dimensions (Gr1 – 1 μm; Gr5 – 5 μm; Gr20 – 20 μm), a graphene oxide (GO – 5 μm), reduced graphene-oxide (rGO – 5 μm), a MWCNT standard that is commonly employed in various previous studies; Mitsui-7 (MW-#5), pristine as-produced MWCNT (MW-#3, MW-#2) and their polymer-coated counterparts (MW-#3-PC, MW-#2-PC) from two different sources, as well as carbon black (CB – is Printex 90 Degussa).

in red and down regulation in blue. Overall, the dendrogram initially divided nanoparticle exposure responses into two clusters or groups, one predominantly containing day 1, and the other containing 28 days post-exposure end points (Figure 1). The first cluster grouped together all 1 d post-exposure carbonaceous nanomaterials except for Gr1. Within this first cluster, a breaking point further divided it into two sub-clusters. The first sub-cluster contained only MW-#2, MW-#2-PC, MW-#3, and MW-#3-PC. Within this sub-cluster, co-clustering between materials was evident. Even though MW-#3 and MW-#3-PC (polymer coated) exhibited co-clustering on the heat map, MW-#3-PC had a much lower fold change value, indicating less inflammatory response from MW-#3. Interestingly, MW-#5 (MWCNT-7), a well-studied material used as a reference, clustered with the graphenes, in particular rGO, rather than other MWCNTs i.e. MW-#3 and MW-#3-PC. This suggests that MW-#3 and MW-#3-PC produce a differential inflammatory response in comparison to MW-#5 and rGO. The second sub-cluster showed Gr20 in close proximity to carbon black (CB) and Gr5 in close proximity to GO at day 1, and rGO in close proximity to MW-#5 at both 1 and 28 d (Figure 1).

The second cluster grouped all day 28 post-exposure carbonaceous nanomaterials close to the control (DM), with the exception of rGO and MW-#5. In addition, a clear distinction between graphene and MW-#3, MW-#3-PC, MW-#2, and MW-#2-PC was also made at this time point (Supplemental Figure S1). The clustering of rGO and MW-#5 at day 28 post-exposure with 1 d post-exposure responses in general suggests a persistence of inflammation similar to that of the acute response even at 28 d in these nanomaterials. Importantly, 19 out of the 46 evaluated proteins were found to differentiate between persistent and resolving inflammatory responses upon exposure to various carbonaceous nanoparticles. Of these 19 proteins, MMP-9, MCP-1, and MCP-3 > IL-6, MIP-1β, and MIP-1γ > TIMP-1 mouse, IP-10, and MCP-5 > IL-18, EGF, GM-CSF, KC/GRO, LIF, MIP-2, MIP-1α, thrombopoietin, eotaxin, and MDC, in that order were highly indicative of differing responses. Overall, HCA suggested the existence of two different groupings of nanomaterials based on their inflammatory responses at 1 and 28 d in BAL fluid: (1) rGO and MW-#5, MW-#3, MW-#3-PC, MW-#2, and MW-#2-PC; (2) GO, Gr20, Gr5, Gr1, and CB (Figure 1 and Supplemental Figure S1).
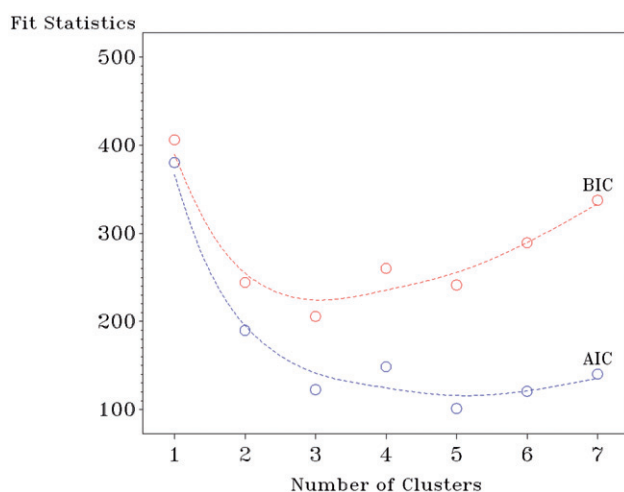
Figure 2. The Akaike Information Criterion (AIC) and the Bayesian Information Criterion (BIC) statistics are plotted for one to seven clusters. The clustering was performed using histopathology data as observed at endpoints of 60 or 84 d of post-exposure to different carbon based nanomaterials investigated.

3.2. LCA grouped together nanoparticles with similar lung pathologies

LCA was performed to identify and categorize nanoparticles based on the sub-types of toxicity responses observed in the lungs (e.g. fibrosis, granulomas, bronchiolitis obliterans). While the obliterans results were considered as binary (yes|no), the fibrosis and granuloma results were further reduced based on minimum/maximum pathological scores in each case, for the purposes of LCA, to the five categories '1' to '5' defined by the following: '1' = 0, '2' = (0–0.5), '3' = (0.5–1), '4' = (1–1.7), and '5' = (>1.7). Figure 2 shows the Akaike Information Criterion (AIC) and the Bayesian Information Criterion (BIC). Independent of the method used both showed local minimums at three clusters. The modeling results for the three-cluster solution are shown in Table 2, and the actual profiles for the three clusters are shown in Table 3, where the profiles are based on the results for the 129 subsamples. In general, Table 3 shows that all of the subsamples in the first cluster were classified into one of the two highest categories of fibrosis and granuloma, and were classified with obliterans. The second and third clusters have no obliterans and are characterized, respectively, by low and middle levels of fibrosis and granuloma. The estimated posterior class probabilities were all greater than 0.98, conditional on the response probabilities found in

Table 2. The parameter estimates and standard errors for the three classes or clusters, the five response categories for granulomas and fibrosis, and the two response categories for obliterans.

Class membership probabilities: gamma estimates (*standard errors*)

Class:	1	2	3
	0.1713	0.4884	0.3403
	0.0796	*0.1046*	*0.0998*

Item response probabilities: Rho estimates (*standard errors*)
Response category 1

	1	2	3
Granuloma:	0.0061	0.839	0.0031
	0.0028	*0.1052*	*0.0009*
Fibrosis:	0.0073	0.9973	0.0037
	0.0033	*0.0006*	*0.0011*
Obliterans:	0.0175	0.9991	0.9984
	0.01	*0.0002*	*0.0005*

Response category 2

	1	2	3
Granuloma:	0.0012	0.1583	0.0006
	0.0005	*0.1052*	*0.0002*
Fibrosis:	0.0014	0.0005	0.272
	0.0006	*0.0001*	*0.165*
Obliterans:	0.9825	0.0009	0.0016
	0.01	*0.0002*	*0.0005*

Item response probabilities: Rho estimates (*standard errors*)
Response category 3

	1	2	3
Granuloma:	0.0015	0.0005	0.2947
	0.0007	*0.0001*	*0.1616*
fibrosis:	0.003	0.001	0.5666
	0.0014	*0.0002*	*0.1393*

Response category 4

	1	2	3
Granuloma:	0.4547	0.0016	0.6556
	0.2108	*0.0003*	*0.1546*
Fibrosis:	0.4968	0.0007	0.157
	0.2336	*0.0002*	*0.069*

Response category 5

	1	2	3
Granuloma:	0.5365	0.0006	0.046
	0.2104	*0.0001*	*0.0427*
Fibrosis:	0.4916	0.0004	0.0006
	0.233	*0.0001*	*0.0002*

Table 2. There are generally small differences between the predicted and actual profiles. For example, the response probabilities for the highest levels of fibrosis and granuloma for the first cluster, found near the bottom of the first column, are estimated as 0.5365 and 0.4916, whereas the actual proportions, calculated for the 129 subsamples, are approximately 0.55 and 0.50. The membership for the three clusters is shown in Table 4. Overall they can be broadly classified into two clusters of particles: (a) those with medium and/or highest

Table 3. The approximate profiles for the three clusters which contain 4, 12, and 8 sampling units.

Condition	Cluster 1 $n = 4$	Cluster 2 $n = 12$	Cluster 3 $n = 8$
Granuloma = 0	0.00	0.84	0.00
Granuloma >0–0.5	0.00	0.16	0.00
Granuloma >0.5–1.0	0.00	0.00	0.30
Granuloma >1.0–1.7	0.45	0.00	0.66
Granuloma >1.7	0.55	0.00	0.05
Fibrosis = 0	0.00	1.00	0.00
Fibrosis >0–0.5	0.00	0.00	0.27
Fibrosis >0.5–1.0	0.00	0.00	0.57
Fibrosis >1.0–1.7	0.50	0.00	0.16
Fibrosis >1.7	0.50	0.00	0.00
No obliterans	0.00	1.00	1.00
Obliterans	1.00	0.00	0.00

The profiles are calculated using the 129 subsamples nested within the 24 samples (12 particles and two different doses investigated).

Table 4. The assignments of the 24 samples to the three different clusters based on Latent Class Analysis of histopathological alterations in the lungs.

Cluster	CNMs
1	MW-#2 and MW-#2-PC
2	CB, Gr1, Gr5, Gr20, and GO
3	MW-#3, MW-#3-PC, MW-#5, and rGO

The dataset consisted of pathological outcomes as observed at day 60 or 84 post-exposure to pristine graphenes of various lateral dimensions (Gr1 – 1 μm; Gr5 – 5 μm; Gr20 – 20 μm), a graphene oxide (GO – 5 μm), reduced graphene-oxide (rGO – 5 μm), a MWCNT standard that is commonly employed in various previous studies; Mitsui-7 (MW-#5), pristine as-produced MWCNT (MW-#3, MW-#2) and their polymer-coated counterparts (MW-#3-PC, MW-#2-PC) from two different sources, as well as carbon black (CB – is Printex 90 Degussa).

categories fibrosis and granuloma – rGO, MW-#5, MW-#3, MW-#3-PC, MW-#2, and MW-#2-PC (Table 4, Cluster #1 and #3); and (b) those that cause no or low fibrosis or granulomas – CB, Gr1, Gr5, Gr20, and GO (Table 4, Cluster #2). This is because fibrosis and granulomatous lesions are most common to all of them including MW-#2 and MW-#2-PC and obliterans is not commonly observed in nanomaterial exposure studies.

3.3. Predictive markers selected that could identify exposure to the groups of carbonaceous nanomaterials

In order to select markers associated with exposure to each group of CNMs based on clustering, we performed a sparse supervised classification algorithm using a binary classification technique. In order to identify protein markers that would specifically predict exposure to each of the two groups of nanomaterials identified from the HCA and LCA, the fold changes of 46 proteins from both vehicle-exposed controls and exposed mice were analyzed

against each other to identify and select markers that can distinguish exposures with high accuracy. High accuracies were indicative of the strong ability of a set of protein markers to predict exposure to the nanomaterials in the tested group. These prediction accuracies are shown in Table 5. Comparing the controls to group 1 yielded a 90.2% accuracy full and 90.8% accuracy testing by using eight proteins selected as optimal for prediction. The eight protein markers selected for this differentiation were eotaxin/CCL11, fibrinogen, FGF-Basic, IL-7, LIF, MDC/CCL22, MIP-3β, and TIMP1-mouse. Comparing the controls to group 2 yielded a slightly lower accuracy of 86.4% for full and 85.5% for testing using 6 selected protein markers, IL-6, M-CSF-1, MDC/CCL22, MIP-1α, MIP-1γ, and MIP-3β, differentiating between samples from mice exposed to group 2 materials and vehicle-exposed controls. Overall, the controls versus group 2 returned the lowest accuracy indicating that the responses upon exposure to CNMs, especially at extended time points, belonging to group 2 could be indistinguishable from controls.

Additionally, it is crucial to understand what inflammatory factors or proteins discriminate between the groups of CNMs that had distinct toxicological and pathological outcomes. In order to select protein markers that discriminate between the two CNM exposure groups (i.e. group 1 versus group 2), the proteins from each group were treated as a single class and analyzed similarly using the sparse classification algorithm. Evaluating group 1 in comparison to group 2 yielded a full accuracy of 87.6% and testing accuracy of 85.6% by using 14 of the 27 proteins selected during pre-filtering. The 14 protein markers were eotaxin/CCL11, fibrinogen, FGF-basic, GH, IL-1β, IL-5, IL-7, IL-11, IL-18, MIP-1α, MIP-3β, PAI-1, VCAM-1, and vWF. Out of 14 protein markers selected, four protein markers (eotaxin-1/CCL11, fibrinogen, FGF-basic, and MIP-3β) and two (MIP-1α and MIP-3β) were part of the markers selected to be distinguishing between vehicle-exposed controls and CNMs belonging to group 2 or group 1, respectively (Figure 3). Further, the predictive power of the three classification models and the selected feature sets were evaluated using test datasets, which was never used in training the models. The prediction accuracy along with performance evaluation measures (e.g.

Table 5. Details of the training and test datasets for building the classification models along with markers selected by the corresponding trained models of each group for optimal classification of the exposure to CNMs belonging to each group from vehicle-exposed (DM) controls and different groups.

Dataset Name (Exposure Method)	Sample Size (Class 1, Class 2)	Feature Size Post t-test	Controls	Time Points	Graphene-based materials	Multi-walled carbon nanotubes	Carbon Black	Accuracy Full (%)	Selected Markers	Accuracy Testing (%)
DM versus group 1	159 (31, 128)	38	DM	24 h, 28 d	rGO	MW-#5, MW-#3, MW-#3-PC, MW-#2, MW-#2-PC	–	90.2	Eotaxin, Fibrinogen, FGF-Basic, IL-7, LIF, TIMP-1, MDC, MIP-3β	90.8
DM versus group 2	132 (31, 101)	32	DM	24 h, 28 d	Gr1, Gr5, Gr20, GO	–	CB	86.4	IL-6, M-CSF-1, MIP-1γ, MIP-1α, MDC, MIP-3β	85.5
Group 1 versus group 2	229 (128, 101)	27	–	24 h, 28 d	rGO, Gr1, Gr20, Gr5, GO	MW-#5, MW-#3, MW-#3-PC, MW-#2, MW-#2-PC	CB	87.6	Eotaxin, FGF-Basic, MIP-1α, MIP-1β, IL-18, vWF, Fibrinogen, IL-7 GH, IL-1β, IL-5, IL-11, PAI-1, VCAM-1	85.6

The reported low- and high-dose levels correspond to 4 μg and 40 μg per mouse for oropharyngeal aspiration exposure. All particles reported had low and high dose levels at days 1 and 28 post-exposure time points with the exception of Gr1, GO, and Gr20, at day 28, which only had data high-dose exposure. Physiological dispersion media or vehicle (DM); Pristine graphenes of various lateral dimensions (Gr1 – 1 μm; Gr5 – 5 μm; Gr20 – 20 μm); a graphene oxide (GO – 5 μm); reduced graphene-oxide (rGO – 5 μm); Mitsui-7 (MW-#5); pristine as-produced MWCNT (MW-#3 and MW-#2) and their polymer-coated counterparts (MW-#3-PC and MW-#2-PC) from two different sources; carbon black (CB – is Printex 90 Degussa).

sensitivity and specificity) is reported in Table 1. Importantly, the selection of set of markers as discriminating features between exposure to groups 1 and 2 resulted in the overall higher accuracy of prediction than the DM versus group 1/group 2 models. Interestingly the specificity, which determines how often the model can truly classify a CNM exposed sample, was 100% in each case irrespective of the overall accuracies (Table 1). This suggests that the identified and selected markers in each case have the potential to serve as predictive markers of exposure to each type of CNM considered as well as can discriminate between CNMs with and without adverse pathological outcomes.

4. Discussion

In this study, we present an approach to group or categorize various CNMs (i.e. multi-walled carbon nanotubes, graphene-based materials, carbon black, and/or their derivatives) based on their altered protein secretion profiles in BALF and pulmonary pathological outcomes following exposure. As a first step, hierarchical cluster analysis was performed to identify subgroups of CNMs with similar pulmonary response profiles using a panel of proteins measured in the BAL fluid at 1 and 28 d post-exposure to each material investigated. Following this, a LCA was performed to show the similarity between protein and pathology based groupings. This allowed us to assign all the CNMs, considered as part of this study, to two toxicologically distinct groups, groups 1 and 2. Finally, a sparse supervised classification algorithm was applied to the data to select protein markers that would distinguish between these two distinct groups, as well as between vehicle-exposed controls versus exposure to set of CNMs segregated under each group.

HCA assigned all the CNMs investigated as part of this study to two distinct groups, groups 1 and 2, based on their inflammatory responses at 1 and 28 d in BAL fluid. While all graphene-based materials, with the exception of reduced graphene-oxide (rGO), along with CB were separated into group 2, the different types of MWCNTs were all grouped together into group 1. However, within group 1, a co-clustering of (a) MW-#3 and MW-#3-PC, (b) MW-#2 and MW-#2-PC, and (c) rGO and MW-#5 was observed, suggesting that MWCNTs with different
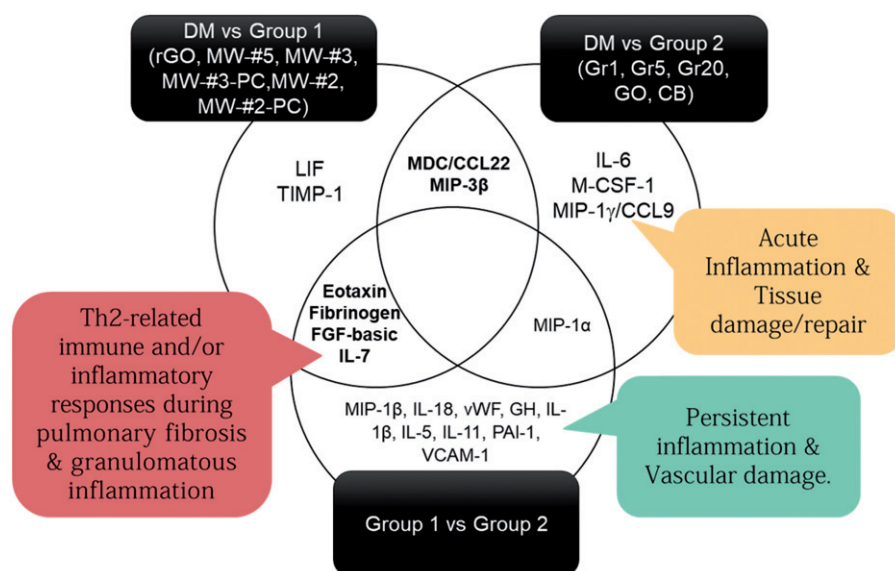
Figure 3. Selected protein markers were found to be extremely predictive of pathological outcomes associated with graphene-based materials, MWCNTs, and carbon black. Successful predictions were attained in the classifier model when comparing group 1 CNMs (rGO, MW-#5, MW-#3, MW-#3-PC,MW-#2, and MW-#2-PC) with group 2 (Gr1, Gr5, Gr20, GO, and CB). Vehicle or physiological dispersion media (DM); Pristine graphenes of various lateral dimensions (Gr1 – 1 μm; Gr5 – 5 μm; Gr20 – 20 μm); a graphene oxide (GO – 5 μm); reduced graphene-oxide (rGO – 5 μm); Mitsui-7 (MW-#5); pristine as-produced MWCNT (MW-#3, MW-#2) and their polymer-coated counterparts (MW-#3-PC, MW-#2-PC) from two different sources; carbon black (CB – is Printex 90 Degussa).

physicochemical properties produce a slightly different inflammatory response. This is further in line with the fact that the properties of these CNMs, even though belonging to the same family of materials, i.e. MWCNTs, are rather different. The LCA-based segregation of CNMs on histological responses including fibrosis, microgranulomas, and proliferative bronchiolitis obliterans also resulted in similar groupings. Importantly, CNMs from group 1 were classified to be belonging to medium and/or highest categories of fibrosis and granuloma (a) without obliterans – rGO, MW-#5, MW-#3 and MW-#3-PC; and (b) with obliterans – MW-#2 and MW-#2-PC. Thus, a possible explanation for the slight separation of MW-#2 and MW-#2-PC within the overall clustering of Group 1 CNMs. In fact, fibrosis and granulomatous lesions were most common to all of Group 1 CNMs including MW-#2 and MW-#2-PC, while obliterans was only observed in MW-#2 and MW-#2-PC exposure studies.

Significantly, two markers, MDC/CCL22 and MIP-3β (Figure 3), were selected as common markers that could distinguish exposure to any of the CNMs from their respective controls investigated as part of this study. Even though MDC was selected as a marker for predicting general pulmonary particulate exposure, a sustained increase in MDC levels (e.g. day 28) was associated only with CNMs belonging to group 1, in particular MW-#3, MW-#3-PC, rGO, and MWCNTs (Figures 1 and Supplemental Figures S1 and S2). Interestingly, a persistent increase in MDC levels over time upon exposure to these CNM materials in this study was correlated with adverse outcomes such as fibrosis and microgranuloma formations (Table 2 and Figures 1 and 2). This is in line with previous studies that found increased MDC/CCL22 in mouse models of human fibrotic lung disease (Belperio et al. 2002), rat radiation pneumonitis/pulmonary fibrosis (Inoue et al. 2004), and rats treated with cigarette smoke (Ritter et al. 2005). Additionally, MDC/CCL22 was also found to be highly elevated in first responders with pulmonary diseases following the 2001 collapse of the World Trade Center (Nolan et al. 2012). Studies evaluating cytokine profile in BALF of lung transplant recipients also showed that the markers identified, i.e. MDC/CCL22 and MIP-3β/CCL19, have been found to be early onset markers predictive of lung failure due to bronchiolitis obliterans syndrome (Meloni et al. 2008). In contrast to group 1 CNMs, exposure to particles such as CB or other group 2 materials resulted in neither fibrosis/microgranuloma

formation nor showed sustained expression of MDC/CCL22 in the lungs over time (Supplemental Figures S1 and S2, compare rGO/MW-#5 with group 2 CNMs at different post-exposure time points).

In addition to MDC/CCL22 and MIP-3β/CCL19, a panel of six protein markers was identified to differentiate between CNM particles of group 1 from group 2 or controls with a high accuracy, shown in Table 5. These protein markers were eotaxin/CCL11, fibrinogen, FGF-basic, LIF, TIMP1$_{mouse}$, and IL-7 (Figure 3). Eotaxin/CCL11, one of the six protein markers identified as discriminating, has the ability to upregulate lung eosinophil and neutrophil accumulation and to increase the expression of profibrogenic cytokines (Huaux et al. 2005). In addition to being an important mediator in eosinophil-mediated inflammatory reactions, eotaxin/CCL11 was shown to regulate neutrophil recruitment into the lungs leading to inflammatory damage (Guo et al. 2001). Similarly, increased levels of eotaxin/CCL11 upon exposure to group 1 particles in this study were inline with the presence of eosinophilic inflammation and accumulation of PMNs in the BAL fluid (Bishop et al. 2017). Additionally, FGF-basic levels was found to be elevated in children with severe community acquired pneumonia, an infection marked by inflammation (Haugen et al. 2015). TIMP-1 expression was found to be up-regulated and associated with fibrogenic responses to bleomycin in rodents (Kim et al. 2005; Manoury et al. 2006; Reinert et al. 2013). IL-7 was found to be linked to early inflammatory responses in the salivary gland, lungs, and liver (Zhou et al. 2015). The selection of eotaxin/CCL11, FGF-basic, TIMP-1, and IL-7 is further supported by the sustained presence of PMN's even after 28 d post-exposure for group 1 particles (Roberts et al. 2015; Bishop et al. 2017). Of the protein markers selected to discriminate group 1 from unexposed controls (Figure 1 and Table 2), eotaxin/CCL11, TIMP-1, and FGF-basic are all chemokines that contribute to T$_h$2-related allergic and immune responses. IL-7, in particular, was reported to accelerate neutrophil recruitment (Wynn 2004; Dong et al. 2016). The detected protein patterns in BAL fluid were able to successfully classify/group different CNM samples, thus establishing a connection between identified protein markers in the BAL fluid to that of lung pathology.

Moreover, a significant increase in the expression of certain cytokines (e.g. MDC/CCL22, eotaxin/CCL11, FGF-basic, TIMP-1, and fibrinogen), selected to predict exposure to group 1 CNMs, were reported to be associated with Th2 granulomatous inflammation and fibrosis (Chiu et al. 2003; Chensue 2013). Notably, exposure to all of the CNM particles in group 1 showed fibrosis and/or granulomatous lesions, albeit with differences in severity (Bishop et al. 2017; Yanamala et al. 2018). In fact, research has shown that FGF-basic, TIMP-1, and fibrinogen have all been found to exacerbate the fibrotic response in interstitial lung diseases (Inoue et al. 1996; Shibata et al. 2013; Giannandrea and Parks 2014). Another study reported increased levels of fibrinogen in granulomatous lesions in horses with chronic pulmonary disease (Winder et al. 1990). LIF also showed levels of elevation in a study of granuloma annulare, suggesting a similar link (Friedman-Birnbaum et al. 1983). Collectively, these findings suggest that the selected protein markers could differentiate CNMs causing persistent inflammation with fibrosis and/or formation of granulomatous lesions in the lungs from exposures that resolved over time. Thus, MDC/CCL22's sustained expression together with other protein markers (e.g. IL-7, FGF-basic, fibrinogen, TIMP-1, etc.) could be critical in classifying CNMs associated with adverse pulmonary outcomes including fibrosis and granulomatous inflammation (Yanamala et al. 2018). Even though proteins such as MMP-9, MCP-1 and MCP-3 were highly overexpressed compared to controls (i.e. DM exposed animals), they were not among the proteins that discriminated neither between each CNM group nor those exposed to CNMs compared to controls (Figure 3). This may because they are either expressed upon exposure to all CNMs belonging to both groups at earlier timepoints (Figure 1) or showed increased levels upon exposure to only certain CNM materials of group 2 at later time points of post-exposure (Supplemental Figures S1 and S2). This could have contributed toward their ability to be identified and selected as proteins that could discriminate biological and pathological responses of exposure to group 1 CNMs from that of group 2 using only days 1 and 28 post-exposure.

Four proteins, IL-6, M-CSF-1, MIP-1α, and MIP-1γ (Figure 3), in addition to eotaxin/CCL11, were selected as protein markers capable of

differentiating between the vehicle-exposed controls and exposure to CNMs of group 2. Group 2 particles showed an acute inflammation albeit with a lack of persistence inflammation at 28 d post-exposure (Figure 1). IL-6, MIP-1α, and MIP-1γ have been found to be heavily associated with the acute inflammatory response, while controlling the development of chronic inflammation by eliciting an immune response. This response is produced by shifting the leukocyte infiltrate from neutrophils to macrophages (Gabay 2006; Krafts 2010). Additionally, IL-6, MIP-1α, MIP-1γ, and M-CSF-1 have been found to be chemoattractants associated with wound healing and repair during tissue damage (Krafts 2010; Jones and Ricardo 2013). Similarly, previous studies have shown the persisting presence of macrophages even after 28 d post-exposure in group 2 particles, particularly graphenes (Roberts et al. 2015; Bishop et al. 2017). This further suggests and supports the ability of these protein markers to discriminate between CNMs belonging to group 2 from controls but not group 1, in particular those that are associated with short-term inflammation which resolves over time.

There have been multiple considerations and suggestions put forth in the literature regarding how to classify and group NMs for safety assessments (Kuempel et al. 2012; Arts et al. 2014; Lynch, Weiss, and Valsami-Jones 2014; Arts et al. 2015, 2016; Riebeling et al. 2017). Based on the physico-chemical properties of CNMs some of them, in particular MWCNTs, could resist clearance and degradation leading to persistence and accumulation in the lungs. Such persistence of particles, some of which have a high aspect ratio, in the lungs can lead to chronic inflammation, interstitial fibrosis, granuloma formation, and carcinogenicity (Poland et al. 2008; Mercer et al. 2011). Fibrosis as a pathological outcome, in particular, is observed in most chronic inflammatory diseases as well as nanomaterial exposures (Wynn 2008; Wynn and Ramalingam 2012). Although typically increased inflammation precedes or coincides with the development of fibrosis, results from a variety of experimental models suggest that fibrosis is not always characterized by intense continued inflammation. This may be due to the shift in the Th1/Th2 cytokine response of the immune cells especially the macrophages found in close proximity of the fibrotic site. Studies investigating the gene expression patterns of fibrotic tissues in Th1/Th2 polarized mice showed markedly different inflammatory response and fibrotic granulomas. While Th1-polarized mice developed small granulomas with less fibrosis, they expressed genes characteristic of tissue damage. In contrast, Th2-polarized mice formed large granulomas with massive collagen deposition and up-regulated genes associated with wound healing (Sandler et al. 2003). This is further corroborated by our study. The proteins that discriminated exposure to group 1 CNMs from group 2 were represented by markers associated with persistent inflammation and vascular damage (Figure 3). This is also inline with the increased risk of vascular diseases associated with idiopathic pulmonary fibrosis. In particular, exposure to CNMs in group 1 was accompanied by enhanced pulmonary fibrosis and granulomatous lesions. Thus, this study identified a set of protein markers with an attempt to facilitate the grouping of NMs based on the correlations found in both BALF inflammatory proteins and pathological manifestations in the lungs. Identification of specific markers predictive of such biological responses, will not only help us understand the process leading to toxicity but can also be applied as a confirmation or screening tool for grouping NPs into toxicologically relevant groups, thus limiting the amount of testing needed for risk assessment of nanomaterials.

Several limitations were inherent to this study. One effect that was not considered as an adverse outcome in this study was the potential for carcinogenicity. Importantly, two materials that were included as part of this study, i.e. MW#5 from group 1 and CB from group 2 CNMs were both reported to induce lung cancer in animal models and designated as group 2B carcinogens, or possibly carcinogenic to humans, by IARC (Heinrich et al. 1995; Mohr et al. 2006; Sargent et al. 2014; Kasai et al. 2015a, 2015b). Such studies are completely absent for graphene-based materials. The necessary data needed to model carcinogenic outcomes including species differences (e.g. rat versus mouse), evaluation of pathological outcomes at longer time-points and lack of studies for certain CNMs, were not within the scope of this study. In the current study, CNMs segregated into group 1, in general, showed a relatively increased hazard when

compared to group 2 CNM materials that were less potent in terms of fibrosis, inflammation and granulomatous lesions in the lungs. These results do suggest that severity/persistence of inflammation or developing pathology may not necessarily be linked to carcinogenicity for the CNMs evaluated. However, having a nanomaterial (i.e. CB) that is classified as 'possibly carcinogenic' for humans in the 'benign' or 'non-hazardous' group (group 2 CNMs) definitely has implications. Thus, care should be taken when interpreting the findings outlined in this paper. The segregation of CNMs into group 2 does not mean they are 'safe' or 'non-hazardous' but rather these CNMs exhibit similarities in the outcomes and endpoints initially inputted in the model. Further studies incorporating various measurements (e.g. cellular influx, cell viability/toxicity responses, DNA damage, changes in genes/proteins, disease markers and other endpoints) to clarify the segregation of CNM materials into different groups and their relationship to specific CNM characteristics.

5. Conclusions

The power of this approach is the opportunity for continued adaptation and inclusion of discriminatory parameters. For example, in this work we considered a single consistent feature (e.g. analyzed protein analytes from lavage) in relationship to pathological outcomes as a proof of concept. As toxicity of NMs can be multi-parametric and typically involves assessing various end-points, the modeling approach described can be broadened to include, for example, other toxicity endpoints (e.g. cell death, DNA damage, and omics profiles) and intrinsic material and function-related properties. However, it would be advantageous if the toxicity endpoints and assessed material properties are harmonized across studies. By creating a decision-making framework for grouping and testing nanomaterials, it was indicated that most likely grouping of nanomaterials will provide preliminary hypotheses as to mode of action while potentially laying the foundation for the development of adverse outcome pathways. Inclusion of a modeling approach, such as the methods described within, has the possibility to predict and prioritize potential mode of action by linking material properties and adverse outcomes.

References

Ahsen, M. E., T. P. Boren, N. K. Singh, B. Misganaw, D. G. Mutch, K. N. Moore, F. J. Backes, et al. 2017. "Sparse Feature Selection for Classification and Prediction of Metastasis in Endometrial Cancer." *BMC Genomics* 18(S3): 233. doi:10.1186/s12864-017-3604-y.

Arts, J. H., M. Hadi, M. A. Irfan, A. M. Keene, R. Kreiling, D. Lyon, M. Maier, et al. 2015. "A Decision-Making Framework for the Grouping and Testing of Nanomaterials (DF4nanoGrouping)." *Regulatory Toxicology and Pharmacology* 71(2): S1–S27. doi:10.1016/j.yrtph.2015.03.007.

Arts, J. H. E., M. Hadi, A. M. Keene, R. Kreiling, D. Lyon, M. Maier, K. Michel, et al. 2014. "A Critical Appraisal of Existing Concepts for the Grouping of Nanomaterials." *Regulatory Toxicology and Pharmacology* 70(2): 492–506. doi:10.1016/j.yrtph.2014.07.025.

Arts, J. H., M. A. Irfan, A. M. Keene, R. Kreiling, D. Lyon, M. Maier, K. Michel, et al. 2016. "Case Studies Putting the Decision-Making Framework for the Grouping and Testing of Nanomaterials (DF4nanoGrouping) into Practice." *Regulatory Toxicology and Pharmacology* 76: 234–261. doi:10.1016/j.yrtph.2015.11.020.

Belperio, J. A., M. Dy, M. D. Burdick, Y. Y. Xue, K. Li, J. A. Elias, and M. P. Keane. 2002. "Interaction of IL-13 and C10 in the Pathogenesis of Bleomycin-Induced Pulmonary Fibrosis." *American Journal of Respiratory Cell and Molecular Biology* 27(4): 419. doi:10.1165/rcmb.2002-0009OC.

Bishop, L., L. Cena, M. Orandle, N. Yanamala, M. M. Dahm, M. E. Birch, D. E. Evans, et al. 2017. "In Vivo Toxicity Assessment of Occupational Components of the Carbon Nanotube Life Cycle to Provide Context to Potential Health Effects." *ACS Nano* 11(9): 8849–8863. doi:10.1021/acsnano.7b03038.

Braakhuis, H. M., A. G. Oomen, and F. R. Cassee. 2016. "Grouping Nanomaterials to Predict Their Potential to Induce Pulmonary Inflammation." *Toxicology and Applied Pharmacology* 299: 3–7. doi:10.1016/j.taap.2015.11.009.

Bradley, P. S., and O. L. Mangasarian. 1998. Feature Selection via Concave Minimization and Support Vector Machines. *Proceedings of the Fifteenth International Conference on Machine Learning*. San Francisco, CA: Morgan Kaufmann Publishers Inc., 82–90.

Chensue, S. W. 2013. "Chemokines in Innate and Adaptive Granuloma Formation." *Frontiers in Immunology* 4: 43.

Chiu, B. C., C. M. Freeman, V. R. Stolberg, E. Komuniecki, P. M. Lincoln, S. L. Kunkel, and S. W. Chensue. 2003. "Cytokine-Chemokine Networks in Experimental Mycobacterial and Schistosomal Pulmonary Granuloma Formation." *American Journal of Respiratory Cell and Molecular Biology* 29(1): 106–116. doi:10.1165/rcmb.2002-0241OC.

Collins, L. M., and S. T. Lanza. 2010. *The Latent Class Model. Latent Class and Latent Transition Analysis*. Hoboken, NJ: Wiley.

Dong, J., X. Yu, D. W. Porter, L. A. Battelli, M. L. Kashon, and Q. Ma. 2016. "Common and Distinct Mechanisms of Induced Pulmonary Fibrosis by Particulate and Soluble Chemical Fibrogenic Agents." *Archives of Toxicology* 90(2): 385–402. doi:10.1007/s00204-015-1589-3.

Friedman-Birnbaum, R., A. Gilhar, S. Haim, and D. T. Golan. 1983. "Leukocyte Inhibitory Factor (LIF) in Granuloma Annulare: A Comparative Study between the Generalized and the Localized Types." *Acta Dermato-Venereologica* 63: 242–243.

Gabay, C. 2006. "Interleukin-6 and Chronic Inflammation." *Arthritis Research & Therapy* 8: S3. doi:10.1186/ar1917.

Giannandrea, M., and W. C. Parks. 2014. "Diverse Functions of Matrix Metalloproteinases during Fibrosis." *Disease Models & Mechanisms* 7(2): 193–203. doi:10.1242/dmm.012062.

Godwin, H., C. Nameth, D. Avery, L. L. Bergeson, D. Bernard, E. Beryt, W. Boyes, et al. 2015. "Nanomaterial Categorization for Assessing Risk Potential to Facilitate Regulatory Decision-Making." *ACS Nano* 9(4): 3409–3417. doi:10.1021/acsnano.5b00941.

Goodman, L. A. 2007. "On the Assignment of Individuals to Latent Classes." *Sociological Methodology* 37(1): 1–22. doi:10.1111/j.1467-9531.2007.00184.x.

Guo, R. F., A. B. Lentsch, R. L. Warner, M. Huber-Lang, J. V. Sarma, T. Hlaing, M. M. Shi, N. W. Lukacs, and P. A. Ward. 2001. "Regulatory Effects of Eotaxin on Acute Lung Inflammatory Injury." *The Journal of Immunology* 166(8): 5208–5218. doi:10.4049/jimmunol.166.8.5208.

Guyon, I., J. Weston, S. Barnhill, and V. Vapnik. 2002. "Gene Selection for Cancer Classification Using Support Vector Machines." *Machine Learning* 46(1/3): 389–422. doi:10.1023/A:1012487302797.

Haugen, J., R. K. Chandyo, K. A. Brokstad, M. Mathisen, M. Ulak, S. Basnet, P. Valentiner-Branth, and T. A. Strand. 2015. "Cytokine Concentrations in Plasma from Children with Severe and Non-Severe Community Acquired Pneumonia." *PLoS One* 10(9): e0138978. doi:10.1371/journal.pone.0138978.

Heinrich, U., R. Fuhst, S. Rittinghausen, O. Creutzenberg, B. Bellmann, W. Koch, and K. Levsen. 1995. "Chronic Inhalation Exposure of Wistar Rats and Two Different Strains of Mice to Diesel Engine Exhaust, Carbon Black, and Titanium Dioxide." *Inhalation Toxicology* 7(4): 533–556. doi:10.3109/08958379509015211.

Huaux, F., M. Gharaee-Kermani, T. Liu, V. Morel, B. Mcgarry, M. Ullenbruch, S. L. Kunkel, J. Wang, Z. Xing, and S. H. Phan. 2005. "Role of Eotaxin-1 (CCL11) and CC Chemokine Receptor 3 (CCR3) in Bleomycin-induced Lung Injury and Fibrosis." *The American Journal of Pathology* 167(6): 1485–1496. doi:10.1016/S0002-9440(10)61235-7.

Inoue, T., S. Fujishima, E. Ikeda, O. Yoshie, N. Tsukamoto, S. Aiso, N. Aikawa, A. Kubo, K. Matsushima, and K. Yamaguchi. 2004. "CCL22 and CCL17 in Rat Radiation Pneumonitis and in Human Idiopathic Pulmonary Fibrosis." *The European Respiratory Journal* 24(1): 49–56. doi:10.1183/09031936.04.00110203.

Inoue, Y., T. E. King, S. S. Tinkle, K. Dockstader, and L. S. Newman. 1996. "Human Mast Cell Basic Fibroblast Growth Factor in Pulmonary Fibrotic Disorders." *The American Journal of Pathology* 149: 2037–2054.

Jones, C. V., and S. D. Ricardo. 2013. "Macrophages and CSF-1: Implications for Development and beyond." *Organogenesis* 9(4): 249–260. doi:10.4161/org.25676.

Kasai, T., Y. Umeda, M. Ohnishi, H. Kondo, T. Takeuchi, S. Aiso, T. Nishizawa, M. Matsumoto, and S. Fukushima. 2015a. "Thirteen-Week Study of Toxicity of Fiber-like Multi-Walled Carbon Nanotubes with Whole-Body Inhalation Exposure in Rats." *Nanotoxicology* 9(4): 413–422. doi:10.3109/17435390.2014.933903.

Kasai, T., Y. Umeda, M. Ohnishi, T. Mine, H. Kondo, T. Takeuchi, M. Matsumoto, and S. Fukushima. 2015b. "Lung Carcinogenicity of Inhaled Multi-Walled Carbon Nanotube in Rats." *Particle and Fibre Toxicology* 13(1): 53. doi:10.1186/s12989-016-0164-2.

Kim, K. H., K. Burkhart, P. Chen, C. W. Frevert, J. Randolph-Habecker, R. C. Hackman, P. D. Soloway, and D. K. Madtes. 2005. "Tissue Inhibitor of Metalloproteinase-1 Deficiency Amplifies Acute Lung Injury in Bleomycin-Exposed Mice." *American Journal of Respiratory Cell and Molecular Biology* 33(3): 271–279. doi:10.1165/rcmb.2005-0111OC.

Krafts, K. P. 2010. "Tissue Repair: The Hidden Drama." *Organogenesis* 6(4): 225–233. doi:10.4161/org.6.4.12555.

Kuempel, E. D., V. Castranova, C. L. Geraci, and P. A. Schulte. 2012. "Development of Risk-Based Nanomaterial Groups for Occupational Exposure Control." *Journal of Nanoparticle Research* 14(9): 1029. doi:10.1007/s11051-012-1029-8.

Lanza, S. T., J. J. Dziak, L. Huang, A. T. Wagner, and L. M. Collins. 2015. Proc LCA & Proc LTA users' guide (Version 1.3.2). *University Park: The Methodology Center*. Penn State.

Lynch, I., C. Weiss, and E. Valsami-Jones. 2014. "A Strategy for Grouping of Nanomaterials Based on Key Physico-

Chemical Descriptors as a Basis for Safer-by-Design NMs." *Nano Today* 9(3): 266–270. doi:10.1016/j.nantod.2014.05.001.

Manoury, B., S. Caulet-Maugendre, I. Guenon, V. Lagente, and E. Boichot. 2006. "TIMP-1 Is a Key Factor of Fibrogenic Response to Bleomycin in Mouse Lung." *International Journal of Immunopathology and Pharmacology* 19(3): 471–487. doi:10.1177/039463200601900303.

Mclachlan, G., and K. Basford. 1988. *Mixture Models: Inference and Applications to Clustering*. New York, USA: Marcel Dekker.

Meinshausen, N., and P. Bühlmann. 2010. "Stability Selection." *Journal of the Royal Statistical Society: Series B (Statistical Methodology)* 72(4): 417–473. doi:10.1111/j.1467-9868.2010.00740.x.

Meloni, F., N. Solari, S. Miserere, M. Morosini, A. Cascina, C. Klersy, E. Arbustini, C. Pellegrini, M. Viganò, and A. M. Fietta. 2008. "Chemokine Redundancy in BOS Pathogenesis. A Possible Role Also for the CC Chemokines: MIP3-Beta, MIP3-Alpha, MDC and Their Specific Receptors." *Transplant Immunology* 18(3): 275–280. doi:10.1016/j.trim.2007.08.004.

Mercer, R. R., A. F. Hubbs, J. F. Scabilloni, L. Wang, L. A. Battelli, S. Friend, V. Castranova, and D. W. Porter. 2011. "Pulmonary Fibrotic Response to Aspiration of Multi-Walled Carbon Nanotubes." *Particle and Fibre Toxicology* 8(1): 21. doi:10.1186/1743-8977-8-21.

Misganaw, B., E. Ahsen, N. Singh, K. A. Baggerly, A. Unruh, M. A. White, and M. Vidyasagar. 2015. "Optimized Prediction of Extreme Treatment Outcomes in Ovarian Cancer." *Cancer Informatics* 14: 45–55. doi:10.4137/CIN.S30803.

Mohr, U., H. Ernst, M. Roller, and F. Pott. 2006. "Pulmonary Tumor Types Induced in Wistar Rats of the So-called "19-dust study." *Experimental and Toxicologic Pathology* 58(1): 13–20. doi:10.1016/j.etp.2006.06.001.

Niosh-Cib-65. 2013. *Occupational Exposure to Carbon Nanotubes and Nanofibers. Current Intelligence Bulletin*. Cincinnati, OH: Department of Health and Human Services, Centers for Disease and Prevention, National Institute for Occupational Safety and Health, 156 pages.

Nolan, A., B. Naveed, A. L. Comfort, N. Ferrier, C. B. Hall, S. Kwon, K. J. Kasturiarachchi, et al. 2012. "Inflammatory Biomarkers Predict Airflow Obstruction after Exposure to World Trade Center Dust." *Chest* 142(2): 412–418. doi:10.1378/chest.11-1202.

Oomen, A. G., P. M. Bos, T. F. Fernandes, K. Hund-Rinke, D. Boraschi, H. J. Byrne, K. Aschberger, et al. 2014. "Concern-Driven Integrated Approaches to Nanomaterial Testing and Assessment–Report of the NanoSafety Cluster Working Group 10." *Nanotoxicology* 8(3): 334–348. doi:10.3109/17435390.2013.802387.

Poland, C. A., R. Duffin, I. Kinloch, A. Maynard, W. A. Wallace, A. Seaton, V. Stone, S. Brown, W. Macnee, and K. Donaldson. 2008. "Carbon Nanotubes Introduced into the Abdominal Cavity of Mice Show Asbestos-like Pathogenicity in a Pilot Study." *Nature Nanotechnology* 3(7): 423–428. doi:10.1038/nnano.2008.111.

R Core Team. 2014. R: A language and environment for statistical computing. R Foundation for Statistical Computing, Vienna, Austria. http://www.R-project.org/.

Reinert, T., C. S. D. R. Baldotto, F. A. P. Nunes, and A. A. D. S. Scheliga. 2013. "Bleomycin-Induced Lung Injury." *Journal of Cancer Research* 2013: 1.

Riebeling, C., H. Jungnickel, A. Luch, and A. Haase. 2017. "Systems Biology to Support Nanomaterial Grouping." *Advances in Experimental Medicine and Biology* 947: 143–171.

Ritter, M., R. Goggel, N. Chaudhary, A. Wiedenmann, B. Jung, A. Weith, and P. Seither. 2005. "Elevated Expression of TARC (CCL17) and MDC (CCL22) in Models of Cigarette Smoke-Induced Pulmonary Inflammation." *Biochemical and Biophysical Research Communications* 334(1): 254–262. doi:10.1016/j.bbrc.2005.06.084.

Roberts, J. R., R. R. Mercer, A. B. Stefaniak, M. S. Seehra, U. K. Geddam, I. S. Chaudhuri, A. Kyrlidis, et al. 2015. "Evaluation of Pulmonary and Systemic Toxicity following Lung Exposure to Graphite Nanoplates: A Member of the Graphene-Based Nanomaterial Family." *Particle and Fibre Toxicology* 13(1): 34. doi:10.1186/s12989-016-0145-5.

Roberts, J., M. Barger, K. Roach, W. Mckinney, T. Chen, S. Friend, R. Mercer, et al. 2018. Toxicological evaluation of graphene nanomaterials that differ in size and oxidative form following pharyngeal aspiration in mice. *9th International Conference on Nanotoxicology*, Neuss, Germany: Nanotox.

Sandler, N. G., M. M. Mentink-Kane, A. W. Cheever, and T. A. Wynn. 2003. "Global Gene Expression Profiles during Acute Pathogen-Induced Pulmonary Inflammation Reveal Divergent Roles for Th1 and Th2 Responses in Tissue Repair." *The Journal of Immunology* 171(7): 3655–3667. doi:10.4049/jimmunol.171.7.3655.

Sargent, L. M., D. W. Porter, L. M. Staska, A. F. Hubbs, D. T. Lowry, L. Battelli, K. J. Siegrist, et al. 2014. "Promotion of Lung Adenocarcinoma following Inhalation Exposure to Multi-Walled Carbon Nanotubes." *Particle and Fibre Toxicology* 11(1): 3. doi:10.1186/1743-8977-11-3.

Sas-Institute. 2004. *SAS/STAT® User's Guide*. Cary, NC: SAS Institute Inc.

Shibata, Y., S. Abe, S. Inoue, A. Igarashi, K. Yamauchi, Y. Aida, H. Kishi, et al. 2013. "Relationship between Plasma Fibrinogen Levels and Pulmonary Function in the Japanese Population: The Takahata Study." *International Journal of Medical Sciences* 10(11): 1530–1536. doi:10.7150/ijms.7256.

Vidyasagar, M. 2014. "Machine Learning Methods in the Computational Biology of Cancer." *Proceedings. Mathematical, Physical, and Engineering Sciences* 470(2167): 20140081. doi:10.1098/rspa.2014.0081.

Winder, N. C., G. Grunig, M. Hermann, and R. Von Fellenberg. 1990. "Fibrin/Fibrinogen in Lungs and Respiratory

Secretions of Horses with Chronic Pulmonary Disease." *American Journal of Veterinary Research* 51: 945–949.

Wynn, T. A. 2004. "Fibrotic Disease and the T(H)1/T(H)2 Paradigm." *Nature Reviews. Immunology* 4(8): 583–594. doi:10.1038/nri1412.

Wynn, T. A. 2008. "Cellular and Molecular Mechanisms of Fibrosis." *The Journal of Pathology* 214(2): 199–210. doi:10.1002/path.2277.

Wynn, T. A., and T. R. Ramalingam. 2012. "Mechanisms of Fibrosis: Therapeutic Translation for Fibrotic Disease." *Nature Medicine* 18: 1028–1040. doi:10.1038/nm.2807.

Yanamala, N., M. S. Orandle, V. K. Kodali, L. Bishop, P. C. Zeidler-Erdely, J. R. Roberts, V. Castranova, and A. Erdely. 2018. "Sparse Supervised Classification Methods Predict and Characterize Nanomaterial Exposures: Independent Markers of MWCNT Exposures." *Toxicologic Pathology* 46(1): 14–27. doi:10.1177/0192623317730575.

Zhou, J., J.-O. Jin, J. Du, and Q. Yu. 2015. "Innate Immune Signaling Induces IL-7 Production, Early Inflammatory Responses, and Sjögren's-Like Dacryoadenitis in C57BL/6 Mice." *Investigative Opthalmology & Visual Science* 56: 7831–7838. doi:10.1167/iovs.15-17368.